IEEE Access
Multidisciplinary | Rapid Review | Open Access Journal

Received September 16, 2019, accepted October 3, 2019, date of publication October 11, 2019, date of current version October 24, 2019.

Digital Object Identifier 10.1109/ACCESS.2019.2946654

The Harmonic Characteristic of the Advanced Synchronous SVPWM Overmodulation Strategy

JIE CHEN[1], (Member, IEEE), RUIZHENG NI[1], TING LI[1], RUICHANG QIU[1], AND ZHIGANG LIU[2]

[1]School of Electrical Engineering, Beijing Jiaotong University, Beijing 100044, China
[2]Beijing Electrical Engineering Technology Research Center, Beijing 100044, China

Corresponding author: Jie Chen (jiechen@bjtu.edu.cn)

This work was supported in part by the Fundamental Research Funds for the Central Universities under Grant 2018JBM055, and in part by the National Key Research and Development Program of China under Grant.2016YFB1200502.

ABSTRACT The speed range of the rail transit traction system is very wide and mostly uses the hybrid pulse width modulation. The traditional hybrid pulse width modulation requires different types of modulation strategies to cooperate in switching, which inevitably leads to current and torque ripple and complicates the modulation strategy. In order to solve this problem, this paper proposed an advanced synchronous SVPWM overmodulation method, which can greatly simplify the entire modulation strategy. The modulation method is theoretically analyzed and its detailed mathematical expressions are obtained in this paper. Based on the mathematical expression, this paper analyzed the harmonics of the advanced synchronous SVPWM overmodulation strategy and compared it with that of SHE-PWM. Finally, the simulation and experimental verification of the modulation method are carried out, which proves that the method has simple and efficient and excellent harmonic characteristic.

INDEX TERMS Rail transit, traction drive, SVPWM, harmonic analysis.

I. INTRODUCTION

Rail transportation in China is developing rapidly. Both high-speed railway and urban rail transit such as subway and light rail are being placed in a stage of booming development. According to statistics, China's high-speed railway has increased to 22,000 kilometers by the end of 2017 [1], [2], which is longer than all the other countries combined. 35 cities have been served by subway in China, with a total of 171 lines and over 5000 kilometers. As the core equipment in rail vehicles, traction system has also been developed vigorously. The traction system has a very wide speed range and sometimes it is required to switch frequently between high speed zone and low speed zone. Meanwhile, two-level voltage type inverters are often used in the traction system, as shown in Fig.1. As a result of the limitation of development level of IGBT devices, the switching frequency of this high-voltage and high-current field usually does not exceed 1 kHz [3], which makes the single modulating strategy unable to meet the speed range and frequent transformation requirements of the traction system, so the hybrid pulse width modulation (PWM) strategy is often needed [4]–[7].

The associate editor coordinating the review of this manuscript and approving it for publication was Zhigang Liu.

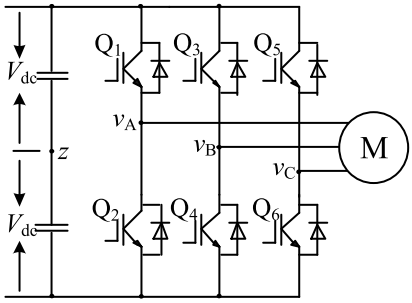

FIGURE 1. Two-level voltage type inverter.

The hybrid PWM strategy can make the traction system run from the asynchronous modulation mode to the six-step mode [7]–[9]. At present, there are two methods for mainstream hybrid PWM, one is: the asynchronous modulation mode - the synchronous modulation mode - the six-step mode [10]–[12], the other is: the asynchronous modulation mode - the synchronous modulation mode - the carrier-free modulation mode - the six-step mode [13]–[15], such as Fig.2. In the first method, the traditional space vector pulse width modulation (SVPWM) or sinusoidal pulse width

This work is licensed under a Creative Commons Attribution 4.0 License. For more information, see http://creativecommons.org/licenses/by/4.0/

modulation (SPWM) + 3rd harmonic injection are used for the asynchronous modulation mode, and the synchronous modulation mode includes the linear modulation region and the overmodulation region [9], [16]–[20]. This method is mostly used by Japanese enterprises, such as Toshiba, Mitsubishi and other companies [21]. The second method differs from the first method because it uses the carrier-free modulation to connect the linear modulation region and the six-step mode region instead of using overmodulation to connect the linear modulation region and the six-step mode region. Here the term carrier-free modulation is referred to selective harmonic elimination pulse width modulation (SHEPWM) [13], [15], [22]–[24] or current harmonic minimum pulse width modulation (CHMPWM) [25]–[28], the principles of these two methods are basically the same, except that the optimized objective function is different. This method is mostly used by European and American enterprises, such as ALSTON, GE and SIEMENS [29].

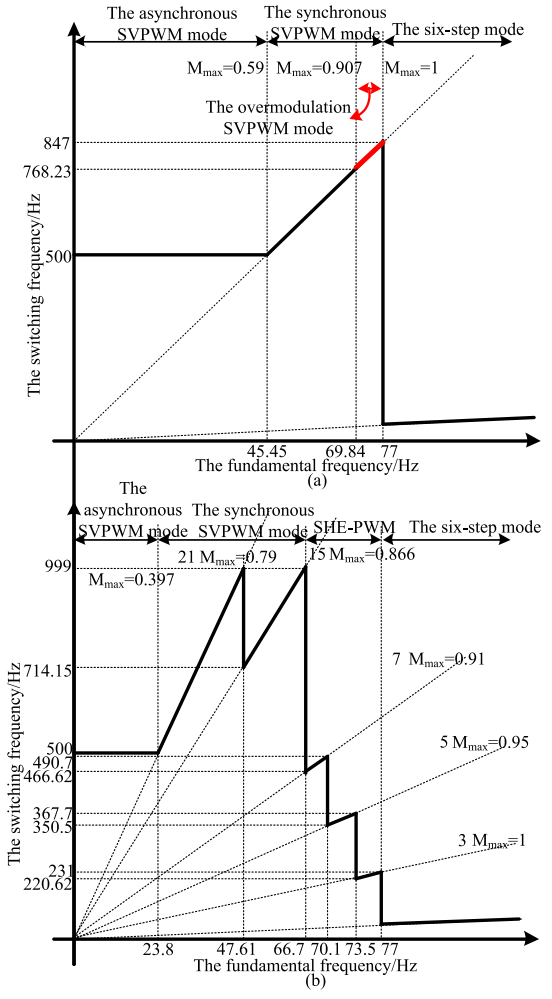

FIGURE 2. **Hybrid PWM strategy in full speed range. (a) The first method. (b) The second method.**

In the hybrid PWM strategy, the switching of different PWM strategies is mainly based on the modulation index (M) and the fundamental frequency, and the fundamental frequency affects the carrier wave ratio. Generally, when the carrier wave ratio N is greater than 15 or 21, the traction system can still adopt the asynchronous modulation. But the carrier ratio N decreases with the increase of the fundamental frequency, and the traction system can only adopt the synchronous modulation. As the modulation index increases further and exceeds 0.907, only overmodulation or carrier-free modulation can be used. When the modulation index reaches 1, the traction system enters the six-step mode.

It is difficult to evaluate the characteristic of the hybrid PWM strategy. There is no evaluation index to evaluate the comprehensive performance of the hybrid PWM strategy so far. The reason is that the hybrid PWM strategy contains multiple modulations, making it complicated and difficult to evaluate comprehensively. However, it is still possible to compare the different hybrid PWM strategies from the severity or ease of implementation and harmonic. Obviously, the first method can be achieved by adopting SVPWM, while the second method requires multiple modulation strategies such as SVPWM and SHE-PWM/CHM-PWM, which involves switching between different modulation strategies, current and torque oscillation are more prone to generate, so the first method is simpler to implement and less prone to generate current and torque oscillation. In addition, except for the overmodulation in the first method and the carrier-free modulation in the second method, the other modulation methods are basically the same, and there is no difference in harmonic characteristic. Therefore the emphasis should be on the harmonic difference of overmodulation and carrier-free modulation.

The common SVPWM overmodulation adopts the two-stage mode [17], [30], [31], which divides into overmodulation region I and the overmodulation region II. In the overmodulation region I, the angle α_r is introduced, when the angle θ of the voltage reference $\vec{V}_{ref}$ (red trajectory) is within [π/6-α_r, π/6+α_r) and [π/2-α_r, π/2), replace $\vec{V}_{ref}$ with $\vec{V}^*_{ref}$ (blue trajectory), at this point $\left|\vec{V}_{ref}\right|$ is less than $\left|\vec{V}^*_{ref}\right|$, when the angle θ of the voltage reference $\vec{V}_{ref}$ (red trajectory) is within [0, π/6-α_r) and [π/6+α_r, π/2-α_r), replace $\vec{V}_{ref}$ with $\vec{V}^*_{ref}$ (blue trajectory), and at this point $\left|\vec{V}_{ref}\right|$ is larger than $\left|\vec{V}^*_{ref}\right|$, as shown in Fig.3 (a). The modulation index of overmodulation region I is between [0.907, 0.9514). In the overmodulation region II, the angle α_h is introduced, when the angle θ of the voltage reference $\vec{V}_{ref}$ (red trajectory) is within [π/6-α_h, π/6+α_h) and [π/2-α_h, π/2), replace $\vec{V}_{ref}$ with $\vec{V}^*_{ref}$ (blue trajectory), at this point $\left|\vec{V}_{ref}\right|$ is less than $\left|\vec{V}^*_{ref}\right|$, when the angle θ of the voltage reference $\vec{V}_{ref}$ (red trajectory) is within [0, π/6-α_h) and [π/6+α_h, π/2-α_h), replace $\vec{V}_{ref}$ with $\vec{V}^*_{ref}$ (blue trajectory), and $\vec{V}^*_{ref}$ is fixed on the vertexes

of the hexagon, as shown in Fig.3 (b). The modulation ratio of overmodulation region I is between [0.9514, 1).

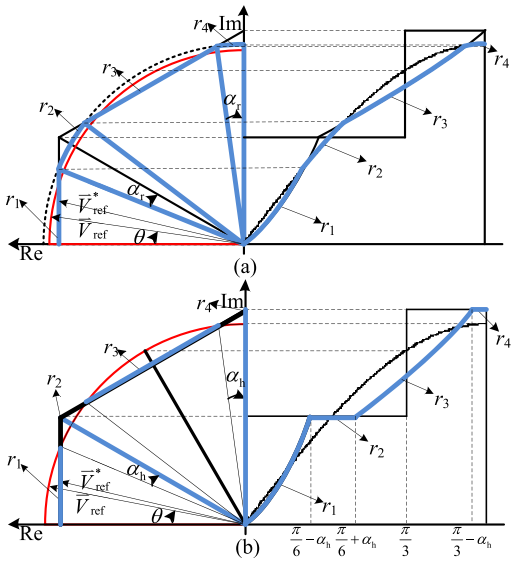

FIGURE 3. SVPWM overmodulation strategy. (a) Overmodulation region I. (b) overmodulation region II.

The above overmodulation strategy with the synchronous modulation can combine into the traditional synchronous SVPWM overmodulation strategy. The traditional synchronous SVPWM overmodulation strategy is widely used, but easier to generate torque oscillation in overmodulation region II. Consequently, Narayanan G advanced the traditional synchronous SVPWM overmodulation strategy. He still divided the whole overmodulation strategy into two regions. Among them, overmodulation region I adopts the same method with the traditional synchronous SVPWM overmodulation strategy. However in the overmodulation region II, he introduced coefficient K, which varied linearly according to the modulation index, and used coefficient K to control voltage vector, reduced current and torque ripple. However, this method still divided the overmodulation into two regions, which makes it complex to implement.

In this paper, an advanced synchronous SVPWM overmodulation strategy (ASSOS) is proposed, which can realize a one-stage transition from the linear modulation to the six-step mode. It is very simple to realize and has good harmonic characteristic. In the second part, ASSOS is proposed. In the third part, the harmonic analysis method of ASSOS is proposed. In the fourth part, the harmonic characteristic of ASSOS and SHE-PWM are compared and analyzed by simulation and experiment, the practicality and excellent harmonic characteristic of ASSOS are proved.

II. THE ADVANCED SYNCHRONOUS SVPWM OVERMODULATION STRATEGY

The traditional SVPWM modulation strategy is based on 8 unit voltage vectors, including 6 active voltage vectors and 2 zero vectors. The 6 active voltage vectors divide the plane into 6 sectors. When the voltage reference runs to a certain sector, the required voltage reference is formed by combining the active voltage vector and the zero vector of the sector. Let the number of vectors in each sector be T, this paper uses $T = 5$ as an example, as shown in Fig.4, $\vec{V}_0 \sim \vec{V}_7$ are the unit voltage vector, and $\vec{U}_1 \sim \vec{U}_5$ are the voltage vector within sector I. With the increase of the modulation index M, the amplitude of the red voltage reference increases gradually, and when the inscribed circle is reached, the traction system transits from the linear modulation to the overmodulation region.

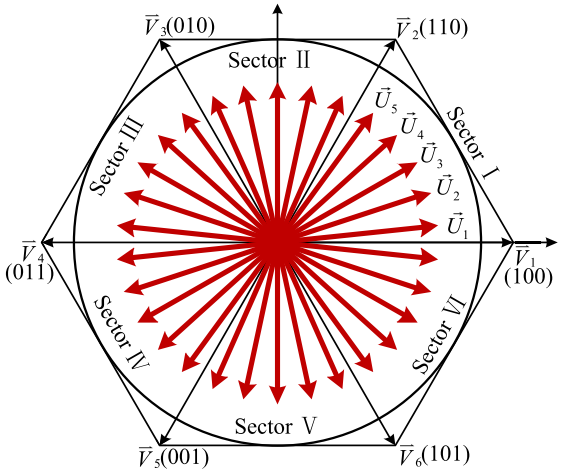

FIGURE 4. Vector graphics of synchronous modulation.

The two-stage overmodulation strategy increases the complexity, but ASSOS simplifies the process, as shown in Fig.5. In the initial stage of the overmodulation, the voltage reference reaches the inscribed circle, and in the final stage the voltage reference is fixed on the vertexes of the hexagon. Therefore, the purpose of the overmodulation is to achieve a smooth transition of the voltage reference from the inscribed circle to the vertexes of the hexagon, and there are myriad transition trajectories theoretically.

In order to realize ASSOS, the whole modulation strategy is divided into two parts: pre-modulation and pulse width calculation, as shown in Fig.6 (a), the pulse width calculation method is consistent with the traditional SVPWM algorithm [32]–[34]. It is better to use the triangular wave as the carrier considering the consistency of the carrier in full speed range, and the switching form of sector I is shown in Fig.6 (b). The purpose of pre-modulation is to achieve a smooth transition of the voltage reference shown in Fig.4 from the inscribed circle to the vertexes of the hexagon, and the modulation index M_i and the angle θ_i for the final modulation are obtained by M and θ (i is the serial number of different pre-modulation methods), below are three common methods, in which the first 30 degrees in sector I are taken as an example.

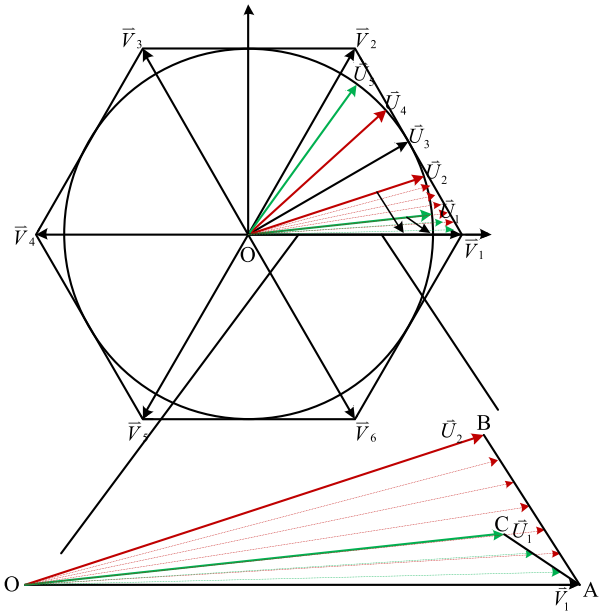

FIGURE 5. The advanced synchronous SVPWM modulation strategy.

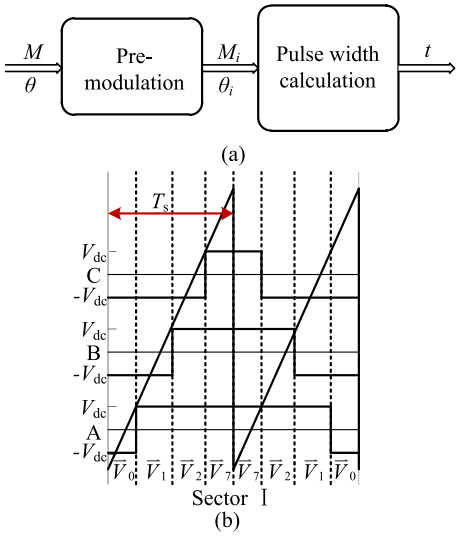

FIGURE 6. The advanced synchronous overmodulation process. (a) Pre-modulation. (b) Switching form in Sector I.

A. THE FIRST METHOD: LINEAR VARIATION OF THE VOLTAGE VECTOR ANGLE AND AMPLITUDE

Introduce the coefficient K, suppose

$$K = \frac{1-M}{1-M_o} \tag{1}$$

where M_o is the critical modulation index of the linear modulation region enter the overmodulation region, which is about 0.907.

Taking the five voltage vectors $\vec{U}_1 \sim \vec{U}_5$ in the sector I as an example, the angle and amplitude of the voltage vector $\vec{U}_1$ and $\vec{U}_2$ trend to $\vec{V}_1$ linearly according to the coefficient K, the angle and amplitude of the voltage vector $\vec{U}_4$ and $\vec{U}_5$ trend to $\vec{V}_2$ linearly according to the coefficient K, $\vec{U}_3$ remains unchanged, and obtain:

$$\angle \vec{U}_2 = K\angle\mathrm{AOB} = \frac{\pi}{10}K \tag{2}$$

$$\left|\vec{U}_2\right| = (\mathrm{AO}-\mathrm{BO})(1-K)+\mathrm{BO} \tag{3}$$

$$\angle \vec{U}_1 = K\angle\mathrm{AOC} = \frac{\pi}{30}K \tag{4}$$

$$\left|\vec{U}_1\right| = (\mathrm{AO}-\mathrm{CO})(1-K)+\mathrm{CO} \tag{5}$$

B. THE SECOND METHOD: LINEAR VARIATION OF THE VOLTAGE VECTOR ANGLE

The coefficient K is introduced and its definition is shown in equation (1). Taking the five voltage vectors $\vec{U}_1 \sim \vec{U}_5$ in the sector I as an example, the angle of the voltage vector $\vec{U}_1$ and $\vec{U}_2$ trend linearly to $\vec{V}_1$ according to the coefficient K, its amplitude is always maintained on AB and AC. Similarly, the voltage vector $\vec{U}_4$ and $\vec{U}_5$ also change in the same way and $\vec{U}_3$ remains unchanged, so we have:

$$\angle \vec{U}_2 = K\angle\mathrm{AOB} = \frac{\pi}{10}K \tag{6}$$

$$\left|\vec{U}_2\right| = \frac{\mathrm{OA}*\sin\angle\mathrm{OAB}}{\sin(\pi-\angle\vec{U}_2-\angle\mathrm{OAB})} \tag{7}$$

$$\angle \vec{U}_1 = K\angle\mathrm{AOC} = \frac{\pi}{30}K \tag{8}$$

$$\left|\vec{U}_1\right| = \frac{\mathrm{OA}*\sin\angle\mathrm{OAC}}{\sin(\pi-\angle\vec{U}_1-\angle\mathrm{OAC})} \tag{9}$$

C. THE THIRD METHOD: LINEAR VARIATION OF DISTANCE BETWEEN VOLTAGE VECTOR AND HEXAGON VERTEXES

The coefficient K is introduced and its definition is shown in equation (1). Taking the five voltage vectors $\vec{U}_1 \sim \vec{U}_5$ in the sector I as an example, the vertex of the voltage vectors $\vec{U}_1$ and $\vec{U}_2$ falls on AC and AB, and its distance from the hexagonal vertexes varies linearly according to the coefficient K. Similarly, the voltage vectors $\vec{U}_4$ and $\vec{U}_5$ change in the same way and $\vec{U}_3$ remains unchanged, therefore:

$$|\vec{U}_2| = \sqrt{\mathrm{OB}^2+[(1-K)\mathrm{AB}]^2-2\mathrm{OB}\cdot[(1-K)\mathrm{AB}]\cdot\cos\angle\mathrm{OBA}} \tag{10}$$

$$\sin\angle\vec{U}_2 = \frac{\sin\angle\mathrm{OAB}}{|\vec{U}_2|}\cdot(K\cdot\mathrm{AB}) \tag{11}$$

$$|\vec{U}_1| = \sqrt{\mathrm{OC}^2+[(1-K)\mathrm{AC}]^2-2\mathrm{OC}\cdot[(1-K)\mathrm{AC}]\cdot\cos\angle\mathrm{OCA}} \tag{12}$$

TABLE 1. Active time of voltage vector.

Sector	Vector	Time	Vector	Time
1 ($0^\circ \le \theta < 60^\circ$)	$\vec{V}_1$ (100)	$\frac{2\sqrt{3}M_1}{\pi}\cos(\theta+\frac{\pi}{6})T_s$	$\vec{V}_2$ (110)	$\frac{2\sqrt{3}M_1}{\pi}\cos(\theta-\frac{\pi}{2})T_s$
2 ($60^\circ \le \theta < 120^\circ$)	$\vec{V}_3$ (010)	$\frac{2\sqrt{3}M_1}{\pi}\cos(\theta-\frac{5\pi}{6})T_s$	$\vec{V}_2$ (110)	$\frac{2\sqrt{3}M_1}{\pi}\cos(\theta-\frac{\pi}{6})T_s$
3 ($120^\circ \le \theta < 180^\circ$)	$\vec{V}_3$ (010)	$\frac{2\sqrt{3}M_1}{\pi}\cos(\theta-\frac{\pi}{2})T_s$	$\vec{V}_4$ (011)	$\frac{2\sqrt{3}M_1}{\pi}\cos(\theta+\frac{5\pi}{6})T_s$
4 ($-180^\circ \le \theta < -120^\circ$)	$\vec{V}_5$ (001)	$\frac{2\sqrt{3}M_1}{\pi}\cos(\theta+\frac{\pi}{2})T_s$	$\vec{V}_4$ (011)	$\frac{2\sqrt{3}M_1}{\pi}\cos(\theta-\frac{5\pi}{6})T_s$
5 ($-120^\circ \le \theta < -60^\circ$)	$\vec{V}_5$ (001)	$\frac{2\sqrt{3}M_1}{\pi}\cos(\theta+\frac{5\pi}{6})T_s$	$\vec{V}_6$ (101)	$\frac{2\sqrt{3}M_1}{\pi}\cos(\theta+\frac{\pi}{6})T_s$
6 ($-60^\circ \le \theta < 0^\circ$)	$\vec{V}_1$ (100)	$\frac{2\sqrt{3}M_1}{\pi}\cos(\theta-\frac{\pi}{6})T_s$	$\vec{V}_6$ (101)	$\frac{2\sqrt{3}M_1}{\pi}\cos(\theta+\frac{\pi}{2})T_s$

$$\sin\angle\vec{U}_1 = \frac{\sin\angle OAC}{|\vec{U}_1|}\cdot(K\cdot AC) \tag{13}$$

The transition trajectories above are just three methods relatively easy to implement of countless methods, they have clear physical interpretation. Compared with the traditional two-stage overmodulation method, this method is much simpler and more efficient, and consumes less chip resources. Compare with the method based on SHE-PWM that require DSP+FPGA dual chip [19], [35], the method requires only a single DSP or SCM, so the development process is greatly shortened.

III. FOURIER ANALYSIS OF THE ADVANCED SYNCHRONOUS SVPWM OVERMODULATION

Harmonic characteristic is an important way to evaluate modulation strategy. Generally, the complex modulation algorithm mostly adopts simulation analysis or actual detection, but it is impossible to analyze the harmonic characteristic of a certain modulation algorithm essentially because these methods cannot obtain its mathematical expression. In this paper, the mathematical expression of ASSOS is detailed derived and obtained, so that the harmonic analysis can be carried out essentially. The basic idea for deriving the mathematical expression of ASSOS is to first determine its modulation wave and then obtain its analytical expression according to the double Fourier analysis method.

Taking the sector I in the first method as an example, the angle and modulation index after pre-modulation can be obtained according to the pre-modulation principle shown in equations (1) ~ (5):

$$M_1 = (\frac{\pi}{3} - \frac{\sqrt{3}\pi}{6})(1-K) + \frac{\sqrt{3}\pi}{6} \tag{14}$$

$$\theta_1 = \begin{cases} K\theta & \theta \le \frac{\pi}{6} \\ \frac{\pi}{3} - K(\frac{\pi}{3} - \theta) & \frac{\pi}{6} < \theta \le \frac{\pi}{3} \end{cases} \tag{15}$$

Equation (15) is only the expression of sector I, the other sectors may have different expressions but they have the same method. The active time of each voltage vector in the six sectors can be obtained according to equations (14) and (15), as show in the following table:

In the table above, T_s is the sampling time.

It can be seen from Fig.6 (b) that the point z of the DC link in Fig.1 is taken as the reference point, and the average value of the voltage of three-phase bridge arm in one sampling period T_s is:

$$v_{az} = V_{dc}(\frac{T_{V_1}}{T_s} + \frac{T_{V_2}}{T_s}) \tag{16}$$

$$v_{bz} = V_{dc}(-\frac{T_{V_1}}{T_s} + \frac{T_{V_2}}{T_s}) \tag{17}$$

$$v_{cz} = V_{dc}(-\frac{T_{V_1}}{T_s} - \frac{T_{V_2}}{T_s}) \tag{18}$$

By substituting the vector active time obtained in Table 1 into equations (16)~(18) then the complete analytical form of the modulation wave in one period of the first method can be obtained, as shown in the following table:

Similarly, analytical expressions of modulation waves of the second method and the third method can be obtained. According to Table 2, the modulation wave of the first method can be drawn. Similarly, the modulation wave of the second method and the third method can also be drawn. The modulation wave of the three methods and the six-step wave are shown in Fig.7. Where the modulation index of the three methods is 0.95.

Similar analysis method of SVPWM modulation in the reference [36] is used, for the terms m≠0, n≠0, the Fourier expression consistent with SVPWM modulation can be given

TABLE 2. The formulation of the phase voltage.

Sector	Phase voltage $v_{az}/\frac{4}{\pi}V_{dc}$ (before 30°)	Phase voltage $v_{az}/\frac{4}{\pi}V_{dc}$ (after 30°)
1 ($0^\circ \le \theta < 60^\circ$)	$v_{az} = M_1' \frac{\sqrt{3}}{2}\cos(K\theta - \frac{\pi}{6})$	$v_{az} = M_1' \frac{\sqrt{3}}{2}\cos[K\theta + \frac{\pi}{3}(1-K) - \frac{\pi}{6}]$
2 ($60^\circ \le \theta < 120^\circ$)	$v_{az} = M_1' \frac{3}{2}\cos[K\theta + (1-K)\frac{\pi}{3}]$	$v_{az} = M_1' \frac{3}{2}\cos[K\theta + (1-K)\frac{2\pi}{3}]$
3 ($120^\circ \le \theta < 180^\circ$)	$v_{az} = M_1' \frac{\sqrt{3}}{2}\cos[K\theta + (1-K)\frac{2\pi}{3} + \frac{\pi}{6}]$	$v_{az} = M_1' \frac{\sqrt{3}}{2}\cos[K\theta + (1-K)\pi + \frac{\pi}{6}]$
4 ($-180^\circ \le \theta < -120^\circ$)	$v_{az} = M_1' \frac{\sqrt{3}}{2}\cos[K\theta + (1-K)\pi - \frac{\pi}{6}]$	$v_{az} = M_1' \frac{\sqrt{3}}{2}\cos[K\theta + (1-K)\frac{4\pi}{3} - \frac{\pi}{6}]$
5 ($-120^\circ \le \theta < -60^\circ$)	$v_{az} = M_1' \frac{3}{2}\cos[K\theta + (1-K)\frac{4\pi}{3}]$	$v_{az} = M_1' \frac{3}{2}\cos[K\theta + (1-K)\frac{5\pi}{3}]$
6 ($-60^\circ \le \theta < 0^\circ$)	$v_{az} = M_1' \frac{\sqrt{3}}{2}\cos[K\theta + (1-K)\frac{5\pi}{3} + \frac{\pi}{6}]$	$v_{az} = M_1' \frac{\sqrt{3}}{2}\cos[K\theta + (1-K)2\pi + \frac{\pi}{6}]$

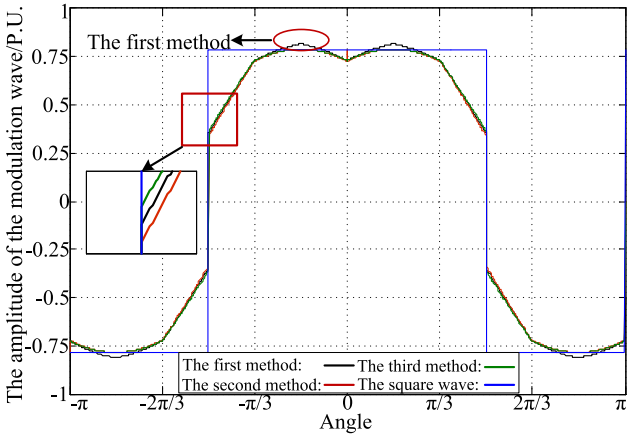

FIGURE 7. Modulation wave of different methods.

as:

$$A_{mn} + jB_{mn} = \frac{V_{dc}}{\pi^2}\sum_{i=1}^{6}\left\{\begin{array}{l}\int_{y_s(i)}^{y_e(i)}\int_{x_r(i)}^{0} e^{j[mx+n(y_r'+\frac{\omega_0}{\omega_c}x+\frac{\omega_0}{\omega_c}\frac{\pi}{2})]}dxdy_r' \\ +\int_{y_s(i)}^{y_e(i)}\int_{x_f(i)}^{0} e^{j[mx+n(y_f'+\frac{\omega_0}{\omega_c}x-\frac{\omega_0}{\omega_c}\frac{\pi}{2})]}dxdy_f'\end{array}\right\} \quad (19)$$

Combining with the characteristic of ASSOS, there are differences in the expression of before and after 30 degrees in each sector, according to Table 2, the boundary conditions of double integral in the above equation can be determined as shown in the following table:

By substituting the boundary conditions in the table above into equation (19). The mathematical expression of ASSOS can be obtained, please see Appendix for calculation details.

IV. THE HARMONICS ANALYSIS OF THE ADVANCED SYNCHRONOUS SVPWM OVERMODULATION

The equation (30) in Appendix is the result of Fourier analysis of ASSOS (the first method). According to which the harmonic characteristic can be analyzed in detail. Two indexes THD and WTHD0 are put forward within the harmonic analysis [36], as shown in equations (20) and (21).

$$THD = \sqrt{\sum_{n=2}^{\infty}(\frac{v_n}{v_1})^2} \quad (20)$$

$$WTHD0 = \frac{\sqrt{\sum_{n=2}^{\infty}(\frac{v_n}{n})^2}}{v_1|_{M=1}} \quad (21)$$

In practical harmonic analysis, we select 30 voltage vectors with a fundamental wave period to analyze, which correspond to $\omega_0/\omega_c = 15$ and the modulation index $M = 0.93$. The spectrums of the first method to the third method are shown in Fig.8∼Fig.10.

It can be seen that THD and WTHD0 of the three synchronous overmodulation strategies are basically the same. At the modulation index of 0.93, THD performance is the best in the first method, followed by the third method and the second method at the end, and for WTHD0 the second method is the best, followed by the first method, and the third method is the last. The reason why the three methods are close in harmonic characteristic is that the three methods have consistent carrier wave and comparison process, only a slight difference in the modulation wave, so the impact on the harmonic characteristic is small. Changing in ranking of

TABLE 3. Boundary conditions.

Sector	$y_s(i)$	$y_e(i)$	$x_r(i)$ (before 30°)	$x_f(i)$ (after 30°)
1	$\frac{5\pi}{6}$	π	$-\frac{\pi}{2}\left[1+M'\frac{\sqrt{3}}{2}\cos[Ky+(1-K)\pi+\frac{\pi}{6}]\right]$	$\frac{\pi}{2}\left[1+M'\frac{\sqrt{3}}{2}\cos[Ky+(1-K)\pi+\frac{\pi}{6}]\right]$
2	$\frac{2\pi}{3}$	$\frac{5\pi}{6}$	$-\frac{\pi}{2}\left[1+M'\frac{\sqrt{3}}{2}\cos[Ky+(1-K)\frac{2\pi}{3}+\frac{\pi}{6}]\right]$	$\frac{\pi}{2}\left[1+M'\frac{\sqrt{3}}{2}\cos[Ky+(1-K)\frac{2\pi}{3}+\frac{\pi}{6}]\right]$
3	$\frac{\pi}{2}$	$\frac{2\pi}{3}$	$-\frac{\pi}{2}\left[1+M'\frac{3}{2}\cos[Ky+(1-K)\frac{2\pi}{3}]\right]$	$\frac{\pi}{2}\left[1+M'\frac{3}{2}\cos[Ky+(1-K)\frac{2\pi}{3}]\right]$
4	$\frac{\pi}{3}$	$\frac{\pi}{2}$	$-\frac{\pi}{2}\left[1+M'\frac{3}{2}\cos[Ky+(1-K)\frac{\pi}{3}]\right]$	$\frac{\pi}{2}\left[1+M'\frac{3}{2}\cos[Ky+(1-K)\frac{\pi}{3}]\right]$
5	$\frac{\pi}{6}$	$\frac{\pi}{3}$	$-\frac{\pi}{2}\left[1+M'\frac{\sqrt{3}}{2}\cos[Ky+\frac{\pi}{3}(1-K)-\frac{\pi}{6}]\right]$	$\frac{\pi}{2}\left[1+M'\frac{\sqrt{3}}{2}\cos[Ky+\frac{\pi}{3}(1-K)-\frac{\pi}{6}]\right]$
6	0	$\frac{\pi}{6}$	$-\frac{\pi}{2}\left[1+M'\frac{\sqrt{3}}{2}\cos(Ky-\frac{\pi}{6})\right]$	$\frac{\pi}{2}\left[1+M'\frac{\sqrt{3}}{2}\cos(Ky-\frac{\pi}{6})\right]$
7	$-\frac{\pi}{6}$	0	$-\frac{\pi}{2}\left[1+M'\frac{\sqrt{3}}{2}\cos(Ky+\frac{\pi}{6})\right]$	$\frac{\pi}{2}\left[1+M'\frac{\sqrt{3}}{2}\cos(Ky+\frac{\pi}{6})\right]$
8	$-\frac{\pi}{3}$	$-\frac{\pi}{6}$	$-\frac{\pi}{2}\left[1+M'\frac{\sqrt{3}}{2}\cos[Ky-\frac{\pi}{3}(1-K)+\frac{\pi}{6}]\right]$	$\frac{\pi}{2}\left[1+M'\frac{\sqrt{3}}{2}\cos[Ky-\frac{\pi}{3}(1-K)+\frac{\pi}{6}]\right]$
9	$-\frac{\pi}{2}$	$-\frac{\pi}{3}$	$-\frac{\pi}{2}\left[1+M'\frac{3}{2}\cos[Ky-\frac{\pi}{3}(1-K)]\right]$	$\frac{\pi}{2}\left[1+M'\frac{3}{2}\cos[Ky-\frac{\pi}{3}(1-K)]\right]$
10	$-\frac{2\pi}{3}$	$-\frac{\pi}{2}$	$-\frac{\pi}{2}\left[1+M'\frac{3}{2}\cos[Ky-\frac{2\pi}{3}(1-K)]\right]$	$\frac{\pi}{2}\left[1+M'\frac{3}{2}\cos[Ky-\frac{2\pi}{3}(1-K)]\right]$
11	$-\frac{5\pi}{6}$	$-\frac{2\pi}{3}$	$-\frac{\pi}{2}\left[1+M'\frac{\sqrt{3}}{2}\cos[Ky-\frac{2\pi}{3}(1-K)-\frac{\pi}{6}]\right]$	$\frac{\pi}{2}\left[1+M'\frac{\sqrt{3}}{2}\cos[Ky-\frac{2\pi}{3}(1-K)-\frac{\pi}{6}]\right]$
12	$-\pi$	$-\frac{5\pi}{6}$	$-\frac{\pi}{2}\left[1+M'\frac{\sqrt{3}}{2}\cos[Ky-\pi(1-K)-\frac{\pi}{6}]\right]$	$\frac{\pi}{2}\left[1+M'\frac{\sqrt{3}}{2}\cos[Ky-\pi(1-K)-\frac{\pi}{6}]\right]$

the second method on the two indices THD and WTHD0 is that although THD is higher in the second method, more harmonics are concentrated in the lower order and the higher harmonics are smaller, so although THD is higher, WTHD0 is smaller.

Fig.8∼Fig.10 only analyse the harmonic characteristic of the three methods at $M = 0.93$. Fig.11 and Fig.12 compare the harmonic characteristic of the three methods in the wide range from the overmodulation region to the six-step mode and compare them with SHE-PWM. It can be seen from the comparison results that the difference between the harmonic characteristic of the three methods in a wide range are still similar to the single point characteristic of $M = 0.93$, and THD of the first method is the best, followed by the third method, and the second method is the last, WTHD0 of the second method is the best, followed by the first method, and the third method is the last. Because the maximum modulation index of 7-pusles SHE-PWM can only be about 0.934, and the maximum modulation index of 5-pulses SHE-PWM can only be about 0.957 [37], THD and WTHD0 in Fig.11 and Fig.12 do no longer change with the modulation index at its high value.

After the traction system enters the high modulation index stage, if the carrier-free modulation strategy such as SHE-PWM is adopted, the number of pulses is usually small, and the carrier wave ratio N is between 3 and 7. In order to compare the harmonic characteristic of ASSOS and SHE-PWM with actual circumstance. It can be seen from the comparison results that since the number of pulses in one fundamental period of ASSOS is more than that of SHE-PWM, even

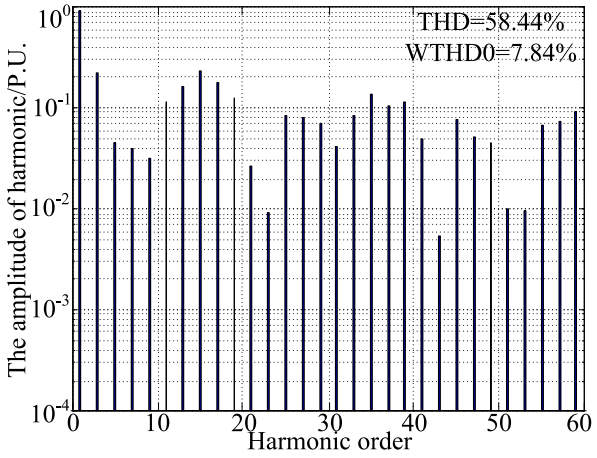

FIGURE 8. The harmonic spectrum of the first method with the modulation index is 0.93.

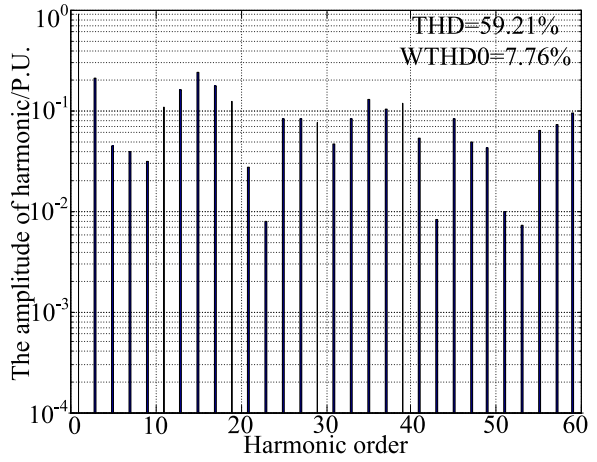

FIGURE 9. The harmonic spectrum of the second method with the modulation index is 0.93.

TABLE 4. Simulated and experimental parameters table.

Motor nominal power/kVA	180	Motor voltage(line-line)/Vrms	550
Stator resistance R_s/Ω	0.0324	Stator inductance L_{ls}/mH	0.72
Rotor resistance R_r/Ω	0.0072	Rotor inductance L_{lr}/mH	0.72
Mutual inductance L_m/H	0.01059	Pole pairs	3
Motor frequency/Hz	77	DC voltage/V	750

though SHE-PWM is specific to optimize for harmonics, the THD characteristic is still not as good as ASSOS, however for WTHD0 characteristic, SHE-PWM has advantage over ASSOS since SHE-PWM eliminates low-order harmonics.

The harmonic analysis indicates that although ASSOS has better THD characteristic than SHE-PWM, the heating in the high speed region of the traction system is slightly higher because the required switching frequency of ASSOS

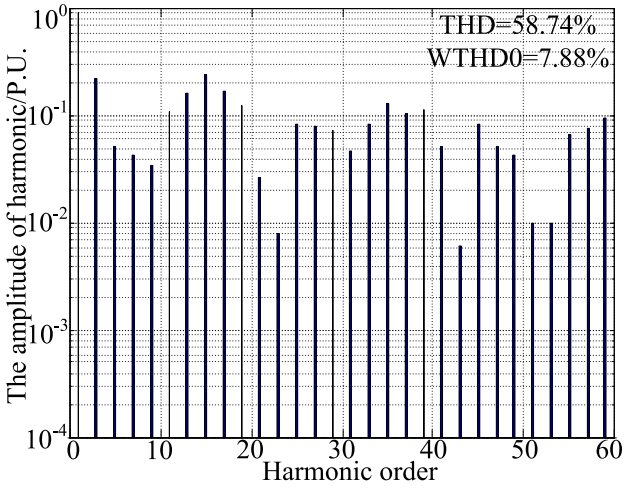

FIGURE 10. The harmonic spectrum of the third method with the modulation index is 0.93.

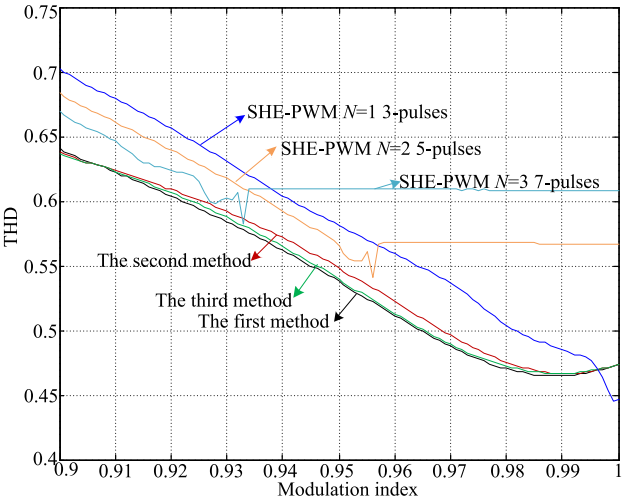

FIGURE 11. The harmonic characteristic of THD.

is higher, which limits the scope of ASSOS to some degree. Generally speaking, the urban rail transit traction system has a lower grade of power than the railway traction system, its switching frequency can reach 1 kHz and ASSOS can be adopted, and the railway traction system can hardly use this modulation mode because its switching frequency is about 500 Hz. However, the implementation of ASSOS is very simple and few hardware resources would be required. The hybrid PWM strategy with ASSOS does not have the problem of switching among different modulation strategies in the full speed range, it can be realized by using a single chip such as DSP, and the hybrid PWM strategy which adopts SHE-PWM needs to switch among different modulation strategies in the full speed range, which requests many more hardware resources and is difficult to implement with a single chip. Usually it adopts the dual-core mode of DSP + FPGA. In addition, the hybrid PWM strategy which adopts ASSOS

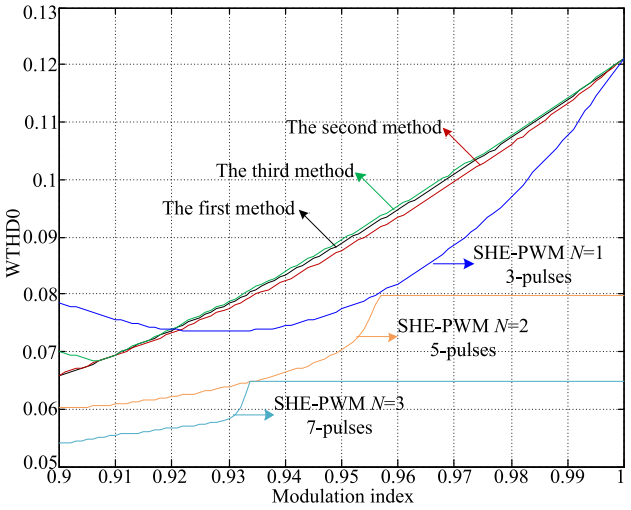

FIGURE 12. The harmonic characteristic of WTHD0.

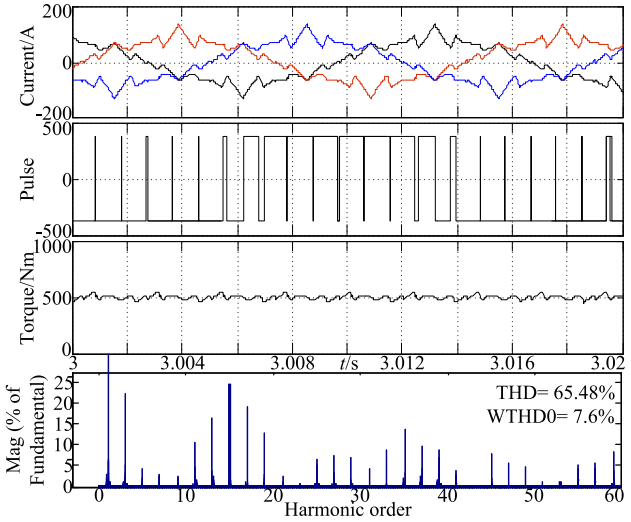

FIGURE 13. The simulation result of the first method.

has the advantage of no torque and current oscillation in switching process because there is no switching between different modulation strategies, which is also an advantage over other hybrid PWM strategies.

As for the three methods, it can be found through comparison that though there is little difference between the three methods in the harmonic characteristic, but that of the first method is slightly better, and the implementation of the first method is also the simplest, with no complex mathematical operations such as trigonometric function and square root, so the first method is an ideal method.

V. SIMULATION AND EXPERIMENT

The stimulated and experimental parameters are shown in the Table 4, this system is applied to Beijing Subway Line 14. The rated voltage of the DC bus of the traction system is 750V, the rated power of the electric motor is 180kVA and the motor frequency is 77Hz. Each traction inverter has

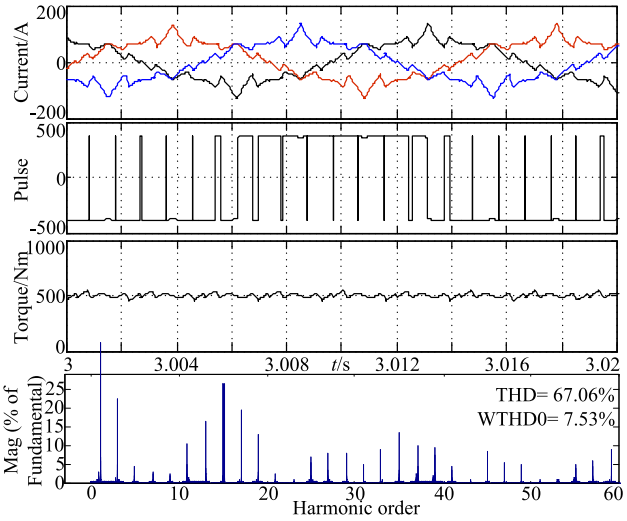

FIGURE 14. The simulation result of the second method.

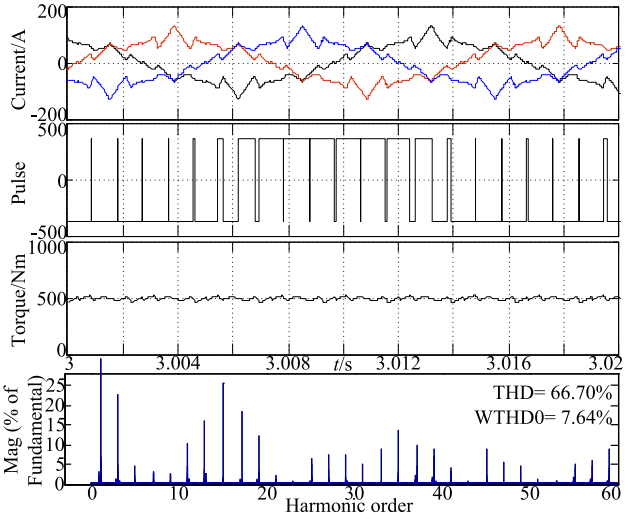

FIGURE 15. The simulation result of the third method.

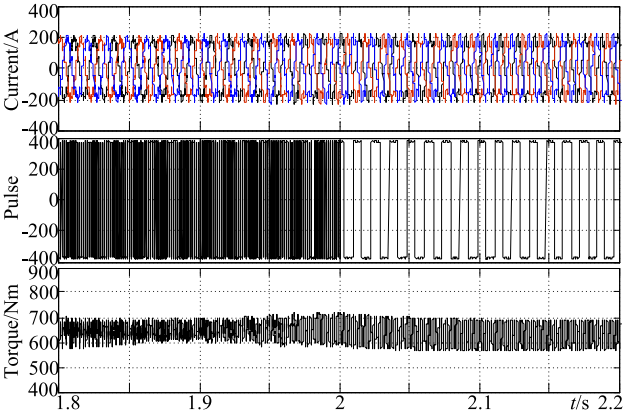

FIGURE 16. Six-step mode simulation result of the third method.

four traction motors. Since the dead-time and limitation of minimum pulse width must be taken into concern in actual

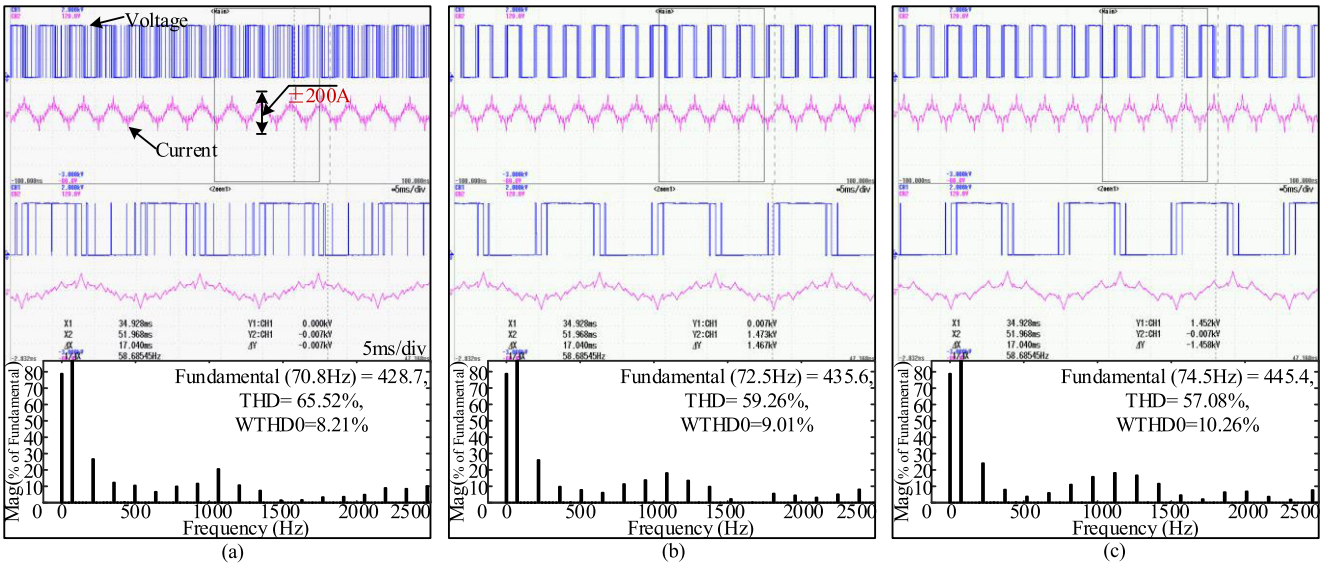

FIGURE 17. The experimental waveforms of the first method. (a) The modulation index is 0.93. (b) The modulation index is 0.95. (c) The modulation index is 0.97.

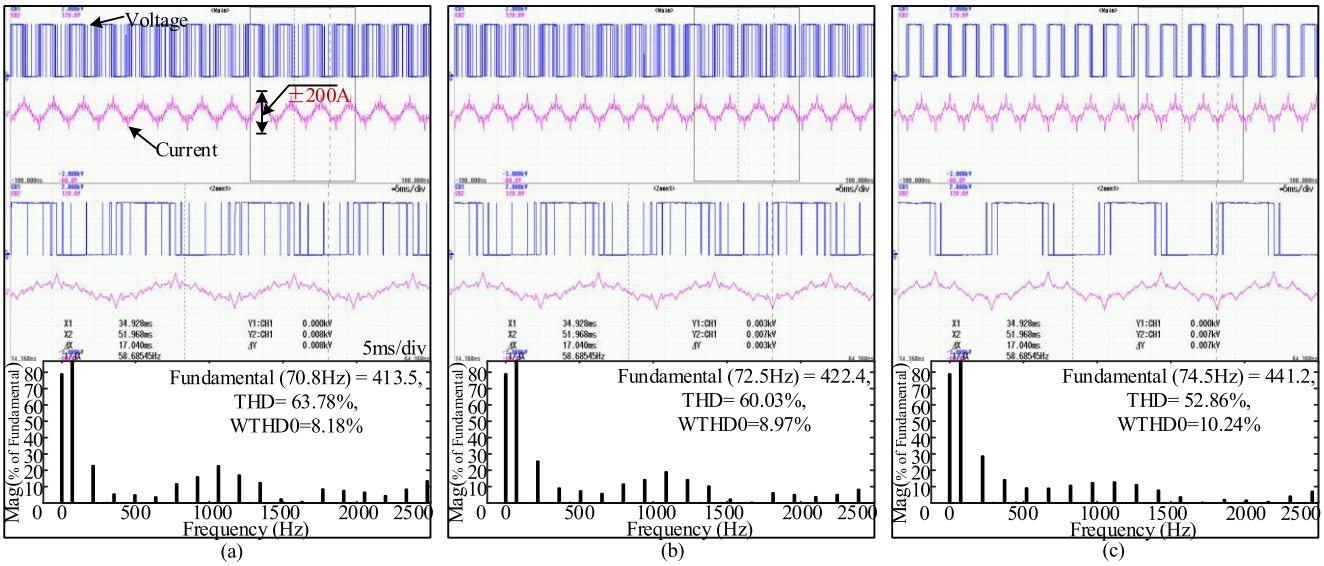

FIGURE 18. The experimental waveforms of the second method. (a) The modulation index is 0.93. (b) The modulation index is 0.95. (c) The modulation index is 0.97.

systems, a dead-time of 3μs and the limitation of minimum pulse width of 10μs have been prescribed, that means the IGBT won't be opened if the pulse width is within10μs.

Fig.13∼Fig.15 are the stimulation waveforms of the first method to the third method respectively, the modulation index is 0.93 and the frequency is 71.61Hz. Compared with the theoretical analysis results, THD obtained by stimulation is higher than the result of theoretical analysis, because in the simulation the limitation of dead-time and minimum pulse width are take into account. The stimulation results show that the characteristic of harmonics of the three methods are basically the same, among which the first method has the best THD characteristic, followed by the second method and the third method is the last. This is similar to the results of stimulation analysis.

As shown in Fig.2 (a), the traction system is always in SVPWM mode in the vast operation range between zero speed to the six-step mode, so there is no problem of switching between different modulation strategies. Fig.16 is the switching stimulation waveform between ASSOS and the six-step mode, it can be seen from the stimulation results that ASSOS can achieve a smooth transition to the six-step mode and without current and torque oscillation.

Fig.17∼Fig.19 are the experimental waveforms of the first method to the third method respectively and the modulation index are 0.93, 0.95 and 0.97 respectively, the experimental

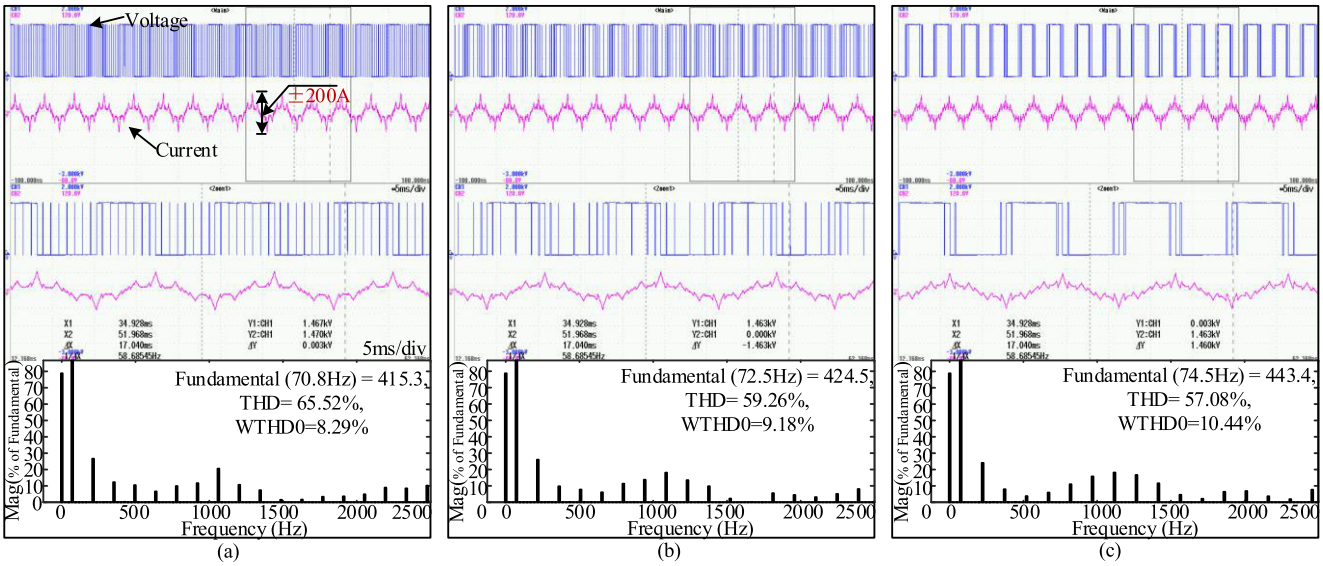

FIGURE 19. The experimental waveforms of the third method. (a) The modulation index is 0.93. (b) The modulation index is 0.95. (c) The modulation index is 0.97.

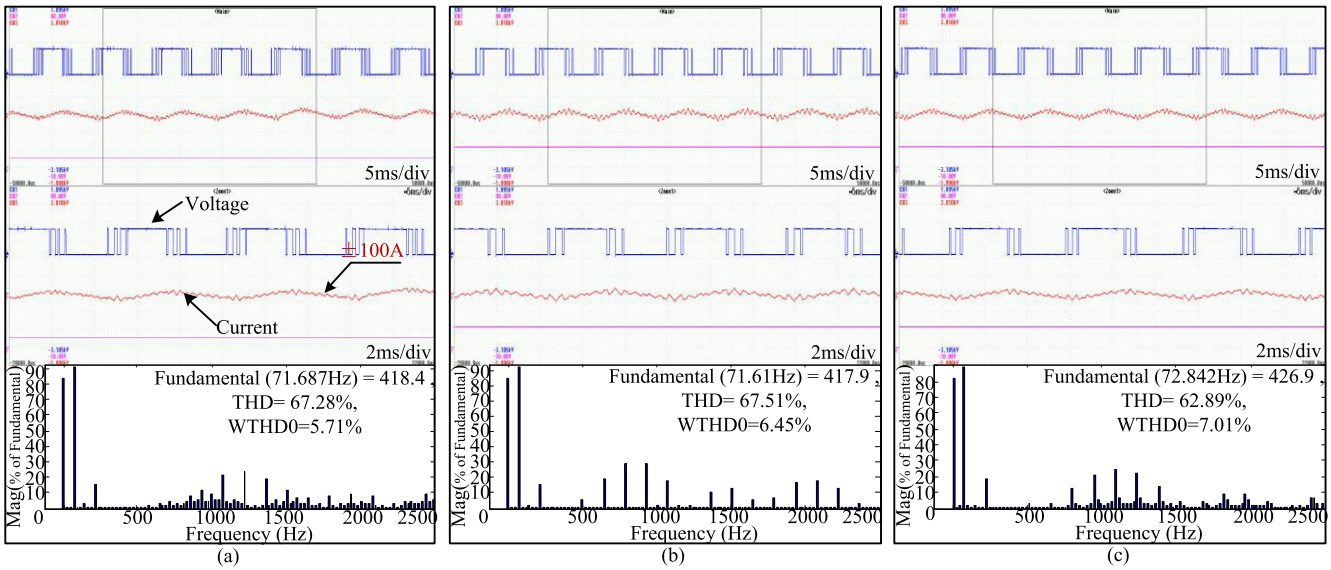

FIGURE 20. The experimental waveforms of 5-pulses SHE-PWM and 7-pulses SHE-PWM. (a) The modulation index of 7-pulses SHE-PWM is 0.93. (b) The modulation index of 5-pulses SHE-PWM is 0.93. (c) The modulation index of 7-pulses SHE-PWM is 0.95.

result is basically consistent with the theoretical analysis, however THD of experimental result is higher than that of stimulation because of the influence of dead-time, limitation of minimum pulse width, IGBT on-off delay, IGBT drop voltage and other factors.

As can be seen from the experimental waveforms, the limitation of minimum pulse width will always intervene under different modulation index, and after that the number of pulse will decrease and the characteristic of THD can be advanced. It can be seen from the experimental results that the harmonics characteristic of the first method is better, which is consistent with the results of stimulation and theoretical analysis.

This paper adopts SHE-PWM under the same traction system and motor conditions in order to compare with ASSOS. SHE-PWM adopts three forms: 7-pulses, 5-pulses and 3-pulses respectively. it can be seen from the THD results that the THD of SHE-PWM is higher than that of ASSOS.

In order to verify the switching features between ASSOS and the six-step mode, this paper adopts the first method in the experiment, as shown in Fig.22. It can be seen from the experimental waveforms that the process of the first method switch to the six-step mode is very smooth and does not generate current oscillation, which is consistent with the theoretical and simulation results.

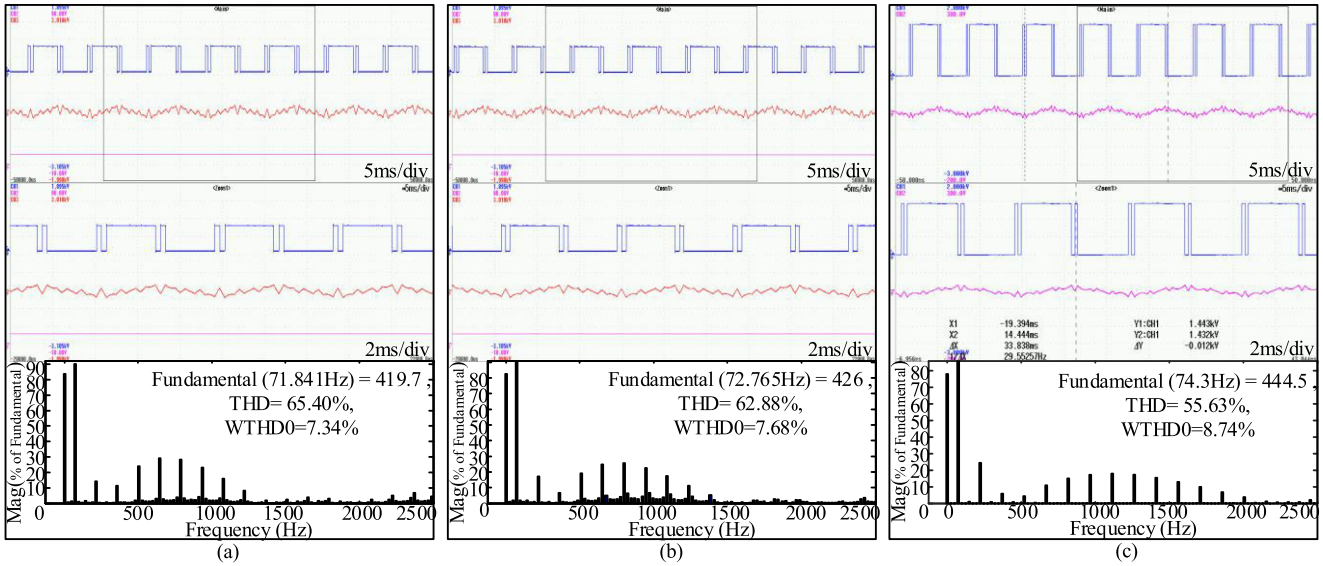

FIGURE 21. The experimental waveforms of the 3-pulses SHE-PWM. (a) The modulation index is 0.93. (b) The modulation index is 0.95. (c) The modulation index is 0.97.

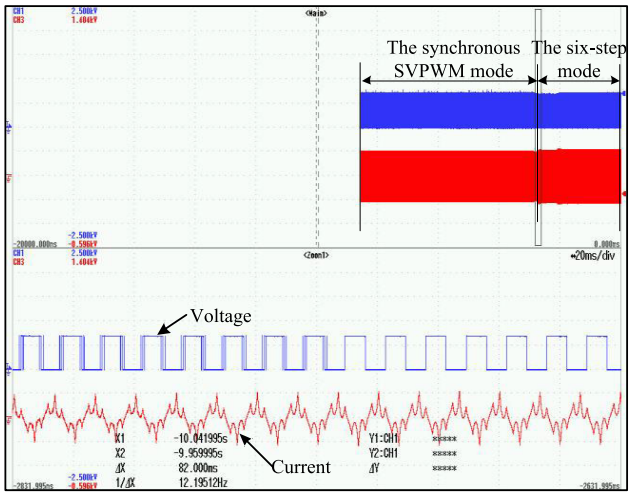

FIGURE 22. The switching experiment from the first method to the six-step mode.

FIGURE 23. The photo of the traction system of Beijing Subway Line 14.

A train on Beijing Subway Line 14 is equipped with our traction system. As shown in Fig.23, the traction system adopts the modulation strategy proposed in this paper, and has been running normally.

VI. CONCLUSION

This paper proposes ASSOS used in the rail transit traction system. This modulation strategy can connect the asynchronous SVPWM mode with the six-step mode, simplify the hybrid PWM strategy in the full speed range of the traction system greatly. In this paper, the mathematical analytic solution of the method is given, and the harmonic characteristic of the method is analyzed. The analysis results show that among the three proposed methods, the harmonic characteristic of the first method is better, but the difference between the three methods is not large, and the THD index of ASSOS is better than SHE-PWM.

APPENDIX

In equation (19), let $q = m + n(\omega_o/\omega_c)$, then:

$$A_{mn} + jB_{mn} = \frac{V_{dc}}{\pi^2} \sum_{i=1}^{6} \left\{ \begin{array}{l} \int_{y_s(i)}^{y_e(i)} \int_{x_r(i)}^{0} e^{jqx} e^{jn(y'_r + \frac{\omega_o}{\omega_c}\frac{\pi}{2})} dx dy'_r \\ + \int_{y_s(i)}^{y_e(i)} \int_{0}^{x_f(i)} e^{jqx} e^{jn(y'_f - \frac{\omega_o}{\omega_c}\frac{\pi}{2})} dx dy'_f \end{array} \right\} \tag{22}$$

After the first multiple integral we find:

$$A_{mn}+jB_{mn}=\frac{V_{\mathrm{dc}}}{jq\pi^2}\sum_{i=1}^{6}\left\{\begin{array}{l}\int_{y_{\mathrm{s}}(i)}^{y_{\mathrm{e}}(i)}e^{jn(y'_{\mathrm{r}}+\frac{\omega_{\mathrm{o}}}{\omega_{\mathrm{c}}}\frac{\pi}{2})}(1-e^{jqx_{\mathrm{r}}(i)})dy'_{\mathrm{r}}\\+\int_{y_{\mathrm{s}}(i)}^{y_{\mathrm{e}}(i)}e^{jn(y'_{\mathrm{f}}-\frac{\omega_{\mathrm{o}}}{\omega_{\mathrm{c}}}\frac{\pi}{2})}(e^{jqx_{\mathrm{f}}(i)}-1)dy'_{\mathrm{f}}\end{array}\right\}\tag{23}$$

Then reorganize and get:

$$A_{mn}+jB_{mn}=\frac{V_{\mathrm{dc}}}{jq\pi^2}\sum_{i=1}^{6}\left\{\begin{array}{l}\int_{y_{\mathrm{s}}(i)}^{y_{\mathrm{e}}(i)}-e^{jny'_{\mathrm{r}}}e^{jn\frac{\omega_{\mathrm{o}}}{\omega_{\mathrm{c}}}\frac{\pi}{2}}e^{jqx_{\mathrm{r}}(i)}dy'_{\mathrm{r}}\\+\int_{y_{\mathrm{s}}(i)}^{y_{\mathrm{e}}(i)}e^{jny'_{\mathrm{f}}}e^{-jn\frac{\omega_{\mathrm{o}}}{\omega_{\mathrm{c}}}\frac{\pi}{2}}e^{jqx_{\mathrm{f}}(i)}dy'_{\mathrm{f}}\end{array}\right\}\tag{24}$$

$$\begin{aligned}A_{mn}+jB_{mn}=&\frac{2V_{\mathrm{dc}}}{q\pi^2}\sum_{i=1}^{12}\\&\times\left\{\begin{array}{l}\int_{y_{\mathrm{s}}(i)}^{y_{\mathrm{e}}(i)}J_0(qM'\frac{\sqrt{3}\pi}{4})\sin m\frac{\pi}{2}e^{jny}+\sum_{k=1}^{\infty}\sin(m+k)\frac{\pi}{2}J_k(qM'\frac{\sqrt{3}\pi}{4})[e^{j[(kK+n)y+k[(1-K)\pi+\frac{\pi}{6}]]}+e^{j[(n-kK)y-k[(1-K)\pi+\frac{\pi}{6}]]}]dy\\+\int_{y_{\mathrm{s}}(i)}^{y_{\mathrm{e}}(i)}J_0(qM'\frac{\sqrt{3}\pi}{4})\sin m\frac{\pi}{2}e^{jny}+\sum_{k=1}^{\infty}\sin(m+k)\frac{\pi}{2}J_k(qM'\frac{\sqrt{3}\pi}{4})[e^{j[(n+kK)y+k[(1-K)\frac{2\pi}{3}+\frac{\pi}{6}]]}+e^{j[(n-kK)y-k[(1-K)\frac{2\pi}{3}+\frac{\pi}{6}]]}]dy\\+\int_{y_{\mathrm{s}}(i)}^{y_{\mathrm{e}}(i)}J_0(qM'\frac{3\pi}{4})\sin m\frac{\pi}{2}e^{jny}+\sum_{k=1}^{\infty}\sin(m+k)\frac{\pi}{2}J_k(qM'\frac{3\pi}{4})[e^{j[(n+kK)y+k[(1-K)\frac{2\pi}{3}]]}+e^{j[(n-kK)y-k[(1-K)\frac{2\pi}{3}]]}]dy\\+\int_{y_{\mathrm{s}}(i)}^{y_{\mathrm{e}}(i)}J_0(qM'\frac{3\pi}{4})\sin m\frac{\pi}{2}e^{jny}+\sum_{k=1}^{\infty}\sin(m+k)\frac{\pi}{2}J_k(qM'\frac{3\pi}{4})[e^{j[(n+kK)y+k[(1-K)\frac{\pi}{3}]]}+e^{j[(n-kK)y-k[(1-K)\frac{\pi}{3}]]}]dy\\+\int_{y_{\mathrm{s}}(i)}^{y_{\mathrm{e}}(i)}J_0(qM'\frac{\sqrt{3}\pi}{4})\sin m\frac{\pi}{2}e^{jny}+\sum_{k=1}^{\infty}\sin(m+k)\frac{\pi}{2}J_k(qM'\frac{\sqrt{3}\pi}{4})[e^{j[(n+kK)y+k[(1-K)\frac{\pi}{3}-\frac{\pi}{6}]]}+e^{j[(n-kK)y-k[(1-K)\frac{\pi}{3}-\frac{\pi}{6}]]}]dy\\+\int_{y_{\mathrm{s}}(i)}^{y_{\mathrm{e}}(i)}J_0(qM'\frac{\sqrt{3}\pi}{4})\sin m\frac{\pi}{2}e^{jny}+\sum_{k=1}^{\infty}\sin(m+k)\frac{\pi}{2}J_k(qM'\frac{\sqrt{3}\pi}{4})[e^{j[(n+kK)y-k\frac{\pi}{6}]}+e^{j[(n-kK)y+k\frac{\pi}{6}]}]dy\\+\int_{y_{\mathrm{s}}(i)}^{y_{\mathrm{e}}(i)}J_0(qM'\frac{\sqrt{3}\pi}{4})\sin m\frac{\pi}{2}e^{jny}+\sum_{k=1}^{\infty}\sin(m+k)\frac{\pi}{2}J_k(qM'\frac{\sqrt{3}\pi}{4})[e^{j[(n+kK)y+k\frac{\pi}{6}]}+e^{j[(n-kK)y-k\frac{\pi}{6}]}]dy\\+\int_{y_{\mathrm{s}}(i)}^{y_{\mathrm{e}}(i)}J_0(qM'\frac{\sqrt{3}\pi}{4})\sin m\frac{\pi}{2}e^{jny}+\sum_{k=1}^{\infty}\sin(m+k)\frac{\pi}{2}J_k(qM'\frac{\sqrt{3}\pi}{4})[e^{j[(n+kK)y+k[-\frac{\pi}{3}(1-K)+\frac{\pi}{6}]]}+e^{j[(n-kK)y-k[-\frac{\pi}{3}(1-K)+\frac{\pi}{6}]]}]dy\\+\int_{y_{\mathrm{s}}(i)}^{y_{\mathrm{e}}(i)}J_0(qM'\frac{3\pi}{4})\sin m\frac{\pi}{2}e^{jny}+\sum_{k=1}^{\infty}\sin(m+k)\frac{\pi}{2}J_k(qM'\frac{3\pi}{4})[e^{j[(n+kK)y-k\frac{\pi}{3}(1-K)]}+e^{j[(n-kK)y+k\frac{\pi}{3}(1-K)]}]dy\\+\int_{y_{\mathrm{s}}(i)}^{y_{\mathrm{e}}(i)}J_0(qM'\frac{3\pi}{4})\sin m\frac{\pi}{2}e^{jny}+\sum_{k=1}^{\infty}\sin(m+k)\frac{\pi}{2}J_k(qM'\frac{3\pi}{4})[e^{j[(n+kK)y-k\frac{2\pi}{3}(1-K)]}+e^{j[(n-kK)y+k\frac{2\pi}{3}(1-K)]}]dy\\+\int_{y_{\mathrm{s}}(i)}^{y_{\mathrm{e}}(i)}J_0(qM'\frac{\sqrt{3}\pi}{4})\sin m\frac{\pi}{2}e^{jny}+\sum_{k=1}^{\infty}\sin(m+k)\frac{\pi}{2}J_k(qM'\frac{\sqrt{3}\pi}{4})[e^{j[(n+kK)y-k[\frac{2\pi}{3}(1-K)+\frac{\pi}{6}]]}+e^{j[(n-kK)y+k[\frac{2\pi}{3}(1-K)+\frac{\pi}{6}]]}]dy\\+\int_{y_{\mathrm{s}}(i)}^{y_{\mathrm{e}}(i)}J_0(qM'\frac{\sqrt{3}\pi}{4})\sin m\frac{\pi}{2}e^{jny}+\sum_{k=1}^{\infty}\sin(m+k)\frac{\pi}{2}J_k(qM'\frac{\sqrt{3}\pi}{4})[e^{j[(n+kK)y-k[\pi(1-K)+\frac{\pi}{6}]]}+e^{j[(n-kK)y+k[\pi(1-K)+\frac{\pi}{6}]]}]dy\end{array}\right\}\end{aligned}\tag{25}$$

$$
\begin{aligned}
&\frac{8V_{\mathrm{dc}}}{\pi^2}\sum_{m=1}^{\infty}\sum_{\substack{n=-\infty\\(n\neq 0)}}^{\infty}\\
&\quad\times\frac{1}{q}\left\{\begin{array}{l}
\frac{\pi}{6}\sin(m+\left|\frac{n}{K}\right|)\frac{\pi}{2}\cos(1-\frac{1}{K})\frac{n\pi}{2}\cos(1-\frac{1}{K})\frac{n\pi}{6}[2J_{|\frac{n}{K}|}(qM'\frac{\sqrt{3}\pi}{4})\cos(\frac{1}{3}-\frac{1}{2K})\pi n+J_{|\frac{n}{K}|}(qM'\frac{3\pi}{4})]\\
+\frac{1}{n}\sin m\frac{\pi}{2}\sin n\frac{\pi}{6}\cos n\frac{\pi}{2}[J_0(qM'\frac{3\pi}{4})-J_0(qM'\frac{\sqrt{3}\pi}{4})]\\
+\sum\limits_{\substack{k=1\\n\neq -kK}}^{\infty}\frac{2}{n+kK}\sin[(n+kK)\frac{\pi}{12}]\sin[(m+k)\frac{\pi}{2}]\cos[(n+kK)\frac{\pi}{2}+k(1-K)\frac{\pi}{2}]\cos\\
[(n+kK)\frac{\pi}{12}+k(1-K)\frac{\pi}{6}][2\cos[(n+kK)\frac{\pi}{3}+k[(1-K)\frac{\pi}{3}+\frac{\pi}{6}]]J_k(qM'\frac{\sqrt{3}\pi}{4})+J_k(qM'\frac{3\pi}{4})]\\
+\sum\limits_{\substack{k=1\\n\neq kK}}^{\infty}\frac{2}{n-kK}\sin[(n-kK)\frac{\pi}{12}]\sin[(m+k)\frac{\pi}{2}]\cos[(n-kK)\frac{\pi}{2}-k(1-K)\frac{\pi}{2}]\cos[(n-kK)\frac{\pi}{12}-k(1-K)\frac{\pi}{6}]\\
[2\cos[(n-kK)\frac{\pi}{3}-k[(1-K)\frac{\pi}{3}+\frac{\pi}{6}]]J_k(qM'\frac{\sqrt{3}\pi}{4})+J_k(qM'\frac{3\pi}{4})]
\end{array}\right\}
\end{aligned}
\tag{29}
$$

$$
\begin{aligned}
v_{\mathrm{an}}(t)&=V_{\mathrm{dc}}+\frac{8V_{\mathrm{dc}}}{\pi^2}\sum_{n=1}^{\infty}\frac{1}{n\frac{\omega_{\mathrm{o}}}{\omega_{\mathrm{c}}}}\\
&\quad\times\left\{\begin{array}{l}
\frac{\pi}{6}\sin(\frac{n}{K})\frac{\pi}{2}\cos(1-\frac{1}{K})\frac{n\pi}{2}\cos(1-\frac{1}{K})\frac{n\pi}{6}[2J_{\frac{n}{K}}(n\frac{\omega_{\mathrm{o}}}{\omega_{\mathrm{c}}}M'\frac{\sqrt{3}\pi}{4})\cos(\frac{1}{3}-\frac{1}{2K})\pi n+J_{\frac{n}{K}}(n\frac{\omega_{\mathrm{o}}}{\omega_{\mathrm{c}}}M'\frac{3\pi}{4})]\\
+\sum\limits_{k=1}^{\infty}\frac{2}{n+kK}\sin[(n+kK)\frac{\pi}{12}]\sin k\frac{\pi}{2}\cos[(n+kK)\frac{\pi}{2}+k(1-K)\frac{\pi}{2}]\cos[(n+kK)\frac{\pi}{12}+k(1-K)\frac{\pi}{6}]\\
[2\cos[(n+kK)\frac{\pi}{3}+k[(1-K)\frac{\pi}{3}+\frac{\pi}{6}]]J_k(n\frac{\omega_{\mathrm{o}}}{\omega_{\mathrm{c}}}M'\frac{\sqrt{3}\pi}{4})+J_k(n\frac{\omega_{\mathrm{o}}}{\omega_{\mathrm{c}}}M'\frac{3\pi}{4})]\\
+\sum\limits_{k=1}^{\infty}\frac{2}{n-kK}\sin[(n-kK)\frac{\pi}{12}]\sin k\frac{\pi}{2}\cos[(n-kK)\frac{\pi}{2}-k(1-K)\frac{\pi}{2}]\cos[(n-kK)\frac{\pi}{12}-k(1-K)\frac{\pi}{6}]\\
[2\cos[(n-kK)\frac{\pi}{3}-k[(1-K)\frac{\pi}{3}+\frac{\pi}{6}]]J_k(n\frac{\omega_{\mathrm{o}}}{\omega_{\mathrm{c}}}M'\frac{\sqrt{3}\pi}{4})+J_k(n\frac{\omega_{\mathrm{o}}}{\omega_{\mathrm{c}}}M'\frac{3\pi}{4})]
\end{array}\right\}\\
&\quad\times\cos n(\omega_{\mathrm{o}}t+\theta_{\mathrm{o}})\\
&\quad+\frac{8V_{\mathrm{dc}}}{\pi^2}\sum_{m=1}^{\infty}\frac{1}{m}\left\{\begin{array}{l}
\frac{\pi}{6}\sin m\frac{\pi}{2}[2J_0(mM'\frac{\sqrt{3}\pi}{4})+J_0(mM'\frac{3\pi}{4})]\\
+\sum\limits_{k=1}^{\infty}\frac{4}{kK}\sin[kK\frac{\pi}{12}]\sin[(m+k)\frac{\pi}{2}]\cos[kK\frac{\pi}{2}+k(1-K)\frac{\pi}{2}]\cos[kK\frac{\pi}{12}+k(1-K)\frac{\pi}{6}]\\
[2\cos[kK\frac{\pi}{3}+k[(1-K)\frac{\pi}{3}+\frac{\pi}{6}]]J_k(mM'\frac{\sqrt{3}\pi}{4})+J_k(mM'\frac{3\pi}{4})]
\end{array}\right\}\\
&\quad\times\cos m(\omega_{\mathrm{c}}t+\theta_{\mathrm{c}})\\
&\quad+\frac{8V_{\mathrm{dc}}}{\pi^2}\sum_{m=1}^{\infty}\sum_{\substack{n=-\infty\\(n\neq 0)}}^{\infty}\\
&\quad\times\frac{1}{q}\left\{\begin{array}{l}
\frac{\pi}{6}\sin(m+\left|\frac{n}{K}\right|)\frac{\pi}{2}\cos(1-\frac{1}{K})\frac{|n|\pi}{2}\cos(1-\frac{1}{K})\frac{|n|\pi}{6}[2J_{|\frac{n}{K}|}(qM'\frac{\sqrt{3}\pi}{4})\cos(\frac{1}{3}-\frac{1}{2K})\pi\,|n|+J_{|\frac{n}{K}|}(qM'\frac{3\pi}{4})]\\
+\frac{1}{n}\sin m\frac{\pi}{2}\sin n\frac{\pi}{6}\cos n\frac{\pi}{2}[J_0(qM'\frac{3\pi}{4})-J_0(qM'\frac{\sqrt{3}\pi}{4})]\\
+\sum\limits_{\substack{k=1\\n\neq -kK}}^{\infty}\frac{2}{n+kK}\sin[(n+kK)\frac{\pi}{12}]\sin[(m+k)\frac{\pi}{2}]\cos[(n+kK)\frac{\pi}{2}+k(1-K)\frac{\pi}{2}]\\
\cos[(n+kK)\frac{\pi}{12}+k(1-K)\frac{\pi}{6}][2\cos[(n+kK)\frac{\pi}{3}+k[(1-K)\frac{\pi}{3}+\frac{\pi}{6}]]J_k(qM'\frac{\sqrt{3}\pi}{4})+J_k(qM'\frac{3\pi}{4})]\\
+\sum\limits_{\substack{k=1\\n\neq kK}}^{\infty}\frac{2}{n-kK}\sin[(n-kK)\frac{\pi}{12}]\sin[(m+k)\frac{\pi}{2}]\cos[(n-kK)\frac{\pi}{2}-k(1-K)\frac{\pi}{2}]\\
\cos[(n-kK)\frac{\pi}{12}-k(1-K)\frac{\pi}{6}][2\cos[(n-kK)\frac{\pi}{3}-k[(1-K)\frac{\pi}{3}+\frac{\pi}{6}]]J_k(qM'\frac{\sqrt{3}\pi}{4})+J_k(qM'\frac{3\pi}{4})]
\end{array}\right\}\\
&\quad\times\cos[n(\omega_{\mathrm{o}}t+\theta_{\mathrm{o}})+m(\omega_{\mathrm{c}}t+\theta_{\mathrm{c}})].
\end{aligned}
\tag{30}
$$

By substituting the integral boundary in Table 3 into equation (24), we can get that (25), as shown at the bottom of the page 13.

First, the first half of each integral in the above formula is summed:

$$\frac{4}{n}\sin m\frac{\pi}{2}\sin n\frac{\pi}{6}\cos n\frac{\pi}{2}[J_0(qM'\frac{3\pi}{4})-J_0(qM'\frac{\sqrt{3}\pi}{4})] \tag{26}$$

$n = |kK|$ and $n \neq |kK|$ need to be considered separately when it comes to sum the second half of each integral in equation (25), when, the second half of each integral in equation (25) is summed and we can get:

$$\begin{aligned}&\frac{2\pi}{3}\sin(m+\left|\frac{n}{K}\right|)\frac{\pi}{2}\cos(\frac{1}{2}-\frac{1}{2K})\pi n\cos(\frac{1}{6}-\frac{1}{6K})\pi n\\&\times[2J_{|\frac{n}{K}|}(qM'\frac{\sqrt{3}\pi}{4})\cos(\frac{1}{3}-\frac{1}{2K})\pi n+J_{|\frac{n}{K}|}\times(qM'\frac{3\pi}{4})]\end{aligned} \tag{27}$$

When $n \neq |kK|$, through a large number of calculations, the summation of the second half of each integral in equation (25) is obtained as follows:

$$\begin{aligned}&\sum_{k=1}^{\infty}\frac{8}{kK+n}\sin(n+kK)\frac{\pi}{12}\sin(m+k)\frac{\pi}{2}\cos[(n+kK)\frac{\pi}{2}\\&+k\frac{\pi}{2}(1-K)]\cos[(n+kK)\frac{\pi}{12}\\&+\frac{k\pi}{6}(1-K)][2\cos[(n+kK)\frac{\pi}{3}\\&+\frac{k}{2}[\pi(1-K)\frac{2k}{3}+\frac{\pi}{3}]]J_k(qM'\frac{\sqrt{3}\pi}{4})+J_k(qM'\frac{3\pi}{4})]\\&+\sum_{k=1}^{\infty}\frac{8}{n-kK}\sin[(n-kK)\frac{\pi}{12}]\sin(m+k)\frac{\pi}{2}\\&\times\cos[(n-kK)\frac{\pi}{2}-k(1-K)\frac{\pi}{2}]\cos\\&\times[(n-kK)\frac{\pi}{12}-k(1-K)\frac{\pi}{6}][2\cos[(n-kK)\frac{\pi}{3}\\&-k[(1-K)\frac{\pi}{3}+\frac{\pi}{6}]]J_k(qM'\\&\times\frac{\sqrt{3}\pi}{4})+J_k(qM'\frac{3\pi}{4})]\end{aligned} \tag{28}$$

Sort out the above calculation results, then gives (29), as shown in the previous page.

Let $m = 0$ and $n = 0$ in the above formulas respectively, and the final result can be obtained (30), as shown in the previous page.

REFERENCES

[1] H. Wang, Z. Liu, A. Núñez, and R. Dollevoet, "Entropy-based local irregularity detection for high-speed railway catenaries with frequent inspections," *IEEE Trans. Instrum. Meas.*, vol. 68, no. 10, pp. 3536–3547, Oct. 2019.

[2] H. Dong, H. Zhu, Y. Li, Y. Lv, S. Gao, Q. Zhang, and B. Ning, "Parallel intelligent systems for integrated high-speed railway operation control and dynamic scheduling," *IEEE Trans. Cybern.*, vol. 48, no. 12, pp. 3381–3389, Dec. 2018.

[3] Z. Zhang, X. Ge, Z. Tian, X. Zhang, Q. Tang, and X. Feng, "A PWM for minimum current harmonic distortion in metro traction PMSM with saliency ratio and load angle constrains," *IEEE Trans. Power Electron.*, vol. 33, no. 5, pp. 4498–4511, May 2018.

[4] V. S. S. P. K. Hari and G. Narayanan, "Space-vector-based hybrid pulse width modulation technique to reduce line current distortion in induction motor drives," *IET Power Electron.*, vol. 5, no. 8, pp. 1463–1471, Sep. 2012.

[5] Z. Wang, B. Wu, D. Xu, and N. R. Zargari, "Hybrid PWM for high-power current-source-inverter-fed drives with low switching frequency," *IEEE Trans. Power Electron.*, vol. 26, no. 6, pp. 1754–1764, Jun. 2011.

[6] Z. Zhang, K. T. Chau, Z. Wang, and W. Li, "Improvement of electromagnetic compatibility of motor drives using hybrid chaotic pulse width modulation," *IEEE Trans. Magn.*, vol. 47, no. 10, pp. 4018–4021, Oct. 2011.

[7] K. Basu, J. S. S. Prasad, G. Narayanan, H. K. Krishnamurthy, and R. Ayyanar, "Reduction of torque ripple in induction motor drives using an advanced hybrid PWM technique," *IEEE Trans. Ind. Electron.*, vol. 57, no. 6, pp. 2085–2091, Jun. 2010.

[8] V. Blasko, "Analysis of a hybrid PWM based on modified space-vector and triangle-comparison methods," *IEEE Trans. Ind. Appl.*, vol. 33, no. 3, pp. 756–764, May/Jun. 1997.

[9] G. Narayanan, D. Zhao, H. K. Krishnamurthy, R. Ayyanar, and V. T. Ranganathan, "Space vector based hybrid PWM techniques for reduced current ripple," *IEEE Trans. Ind. Electron.*, vol. 55, no. 4, pp. 1614–1627, Apr. 2008.

[10] M. Aravind and T. Bhattacharya, "FPGA based Synchronized Sinusoidal Pulse Width Modulation with smooth transition into overmodulation and six step modes of operation for three phase AC motor drives," in *Proc. IEEE Int. Conf. Power Electron. Drives Energy Syst. (PEDES)*, Bengaluru, India, Dec. 2012, pp. 1–6.

[11] J. Holtz, "Pulsewidth modulation for electronic power conversion," *Proc. IEEE*, vol. 82, no. 8, pp. 1194–1214, Aug. 1994.

[12] J. Holtz and N. Oikonomou, "Synchronous optimal pulsewidth modulation and stator flux trajectory control for medium-voltage drives," *IEEE Trans. Ind. Appl.*, vol. 43, no. 2, pp. 600–608, Mar. 2007.

[13] Z. Zhao, Y. Zhong, H. Gao, L. Yuan, and T. Lu, "Hybrid selective harmonic elimination PWM for common-mode voltage reduction in three-level neutral-point-clamped inverters for variable speed induction drives," *IEEE Trans. Ind. Electron.*, vol. 27, no. 3, pp. 1152–1158, Mar. 2012.

[14] A. Maheshwari and K. D. T. Ngo, "Synthesis of six-step pulsewidth-modulated waveforms with selective harmonic elimination," *IEEE Trans. Power Electron.*, vol. 8, no. 4, pp. 554–561, Oct. 1993.

[15] D. Ahmadi, K. Zou, C. Li, Y. Huang, and J. Wang, "A universal selective harmonic elimination method for high-power inverters," *IEEE Trans. Power Electron.*, vol. 26, no. 10, pp. 2743–2752, Oct. 2011.

[16] M. Z. Youssef, K. Woronowicz, K. Aditya, N. A. Azeez, and S. S. Williamson, "Design and development of an efficient multilevel DC/AC traction inverter for railway transportation electrification," *IEEE Trans. Power Electron.*, vol. 31, no. 4, pp. 3036–3042, Apr. 2016.

[17] S. Li, W. Chen, Y. Yan, T. Shi, and C. Xia, "A multimode space vector overmodulation strategy for ultrasparse matrix converter with improved fundamental voltage transfer ratio," *IEEE Trans. Power Electron.*, vol. 33, no. 8, pp. 6782–6793, Aug. 2018.

[18] J. Holtz and X. Qi, "Optimal control of medium-voltage drives—An overview," *IEEE Trans. Ind. Electron.*, vol. 60, no. 12, pp. 5472–5481, Dec. 2013.

[19] M. Hamouda, H. F. Blanchette, K. Al-Haddad, and F. Fnaiech, "An efficient DSP-FPGA-based real-time implementation method of SVM algorithms for an indirect matrix converter," *IEEE Trans. Ind. Electron.*, vol. 58, no. 11, pp. 5024–5031, Nov. 2011.

[20] D. Zhao, V. S. S. P. K. Hari, G. Narayanan, and R. Ayyanar, "Space-vector-based hybrid pulsewidth modulation techniques for reduced harmonic distortion and switching loss," *IEEE Trans. Power Electron.*, vol. 25, no. 3, pp. 760–774, Mar. 2010.

[21] T. Ando, T. Tanamachi, E. Toyota, K. Nakata, M. Suzuki, and K. Yasuda, "Apparatus and method for controlling induction motor," U.S. Patent 6 166 514 A, Dec. 26, 2000.

[22] M. S. A. Dahidah and V. G. Agelidis, "Selective harmonic elimination PWM control for cascaded multilevel voltage source converters: A generalized formula," *IEEE Trans. Power Electron.*, vol. 23, no. 4, pp. 1620–1630, Jul. 2008.

[23] H. S. Patel and R. G. Hoft, "Generalized techniques of harmonic elimination and voltage control in Thyristor inverters: Part I–harmonic elimination," *IEEE Trans. Ind. Appl.*, vol. IA-9, no. 3, pp. 310–317, May 1973.

[24] H. S. Patel and R. G. Hoft, "Generalized techniques of harmonic elimination and voltage control in Thyristor inverters: Part II — Voltage control techniques," *IEEE Trans. Ind. Appl.*, vol. IA-10, no. 5, pp. 666–673, Sep. 1974.
[25] Y. Zhang, Y. W. Li, N. R. Zargari, and Z. Cheng, "Improved selective harmonics elimination scheme with online harmonic compensation for high-power PWM converters," *IEEE Trans. Power Electron.*, vol. 30, no. 7, pp. 3508–3517, Jul. 2015.
[26] J. R. Wells, B. M. Nee, P. L. Chapman, and P. T. Krein, "Selective harmonic control: A general problem formulation and selected solutions," *IEEE Trans. Power Electron.*, vol. 20, no. 6, pp. 1337–1345, Nov. 2005.
[27] J. Napoles, J. I. Leon, R. Portillo, L. G. Franquelo, and M. A. Aguirre, "Selective harmonic mitigation technique for high-power converters," *IEEE Trans. Ind. Electron.*, vol. 57, no. 7, pp. 2315–2323, Jul. 2010.
[28] L. G. Franquelo, J. Napoles, R. C. P. Guisado, J. I. Leon, and M. A. Aguirre, "A flexible selective harmonic mitigation technique to meet grid codes in three-level PWM converters," *IEEE Trans. Ind. Electron.*, vol. 54, no. 6, pp. 3022–3029, Dec. 2007.
[29] B. K. Bose and H. A. Sutherland, "A high-performance pulsewidth modulator for an inverter-fed drive system using a microcomputer," *IEEE Trans. Ind. Appl.*, vol. IA-19, no. 2, pp. 235–243, Mar. 1983.
[30] M. Priestley, J. E. Fletcher, and C. Tan, "Space-vector PWM technique for five-phase open-end winding PMSM drive operating in the overmodulation region," *IEEE Trans. Ind. Electron.*, vol. 65, no. 9, pp. 6816–6827, Sep. 2018.
[31] A. Tripathi, A. M. Khambadkone, and S. K. Panda, "Dynamic control of torque in overmodulation and in the field weakening region," *IEEE Trans. Power Electron.*, vol. 21, no. 4, pp. 1091–1098, Jul. 2006.
[32] H. W. van der Broeck, H.-C. Skudelny, and G. V. Stanke, "Analysis and realization of a pulsewidth modulator based on voltage space vectors," *IEEE Trans. Ind. Appl.*, vol. 24, no. 1, pp. 142–150, Jan. 1988.
[33] S. Lakhimsetty, N. Surulivel, and V. T. Somasekhar, "Improvised SVPWM strategies for an enhanced performance for a four-level open-end winding induction motor drive," *IEEE Trans. Ind. Electron.*, vol. 64, no. 4, pp. 2750–2759, Apr. 2017.
[34] C. Wang, K. Wang, and X. You, "Research on synchronized SVPWM strategies under low switching frequency for six-phase VSI-fed asymmetrical dual stator induction machine," *IEEE Trans. Ind. Electron.*, vol. 63, no. 11, pp. 6767–6776, Nov. 2016.
[35] R. Morales-Caporal, E. Bonilla-Huerta, C. Hernandez, M. A. Arjona, and M. Pacas, "Transducerless acquisition of the rotor position for predictive torque controlled PM synchronous machines based on a DSP-FPGA digital system," *IEEE Trans. Ind. Informat.*, vol. 9, no. 2, pp. 799–807, May 2013.
[36] D. G. Homes and T. A. Lipo, *Pulse Width Modulation for Power Converters: Principles and Practice*, 1st ed. New York, NY, USA: Wiley, 2003.
[37] M. Sharifzadeh, H. Vahedi, and K. Al-Haddad, "New constraint in SHE-PWM for single-phase inverter applications," *IEEE Trans. Ind. Appl.*, vol. 54, no. 5, pp. 4554–4562, Sep/Oct. 2018.

JIE CHEN was born in Zhejiang, China, in 1986. He received the B.S. degree and Ph.D. degrees in electrical engineering and automation from Beijing Jiaotong University, Beijing, China, in 2008 and 2013, respectively.

Since 2013, he has been a Postdoctoral Researcher with Beijing Jiaotong University, Beijing, China, and also with the Institute of Electrical Engineering, Chinese Academy of Sciences, Beijing. He was a Visiting Scholar of WEMPEC with the University of Madison. He is currently an Associate Professor with Beijing Jiaotong University. His research interests include variable frequency drive, rail transportation traction control, and inverter parallel control.

RUIZHENG NI was born in Shanxi, China, in 1994. He received the B.S. degree in electrical engineering and automation from Shanxi Agriculture University, Shanxi, China, in 2016.

Since 2016, he has been a Doctoral Researcher with Beijing Jiaotong University, Beijing, China. His current research interests include transformer lifetime prediction, electric traction, and transmission control.

TING LI was born in Anhui, China, in 1994. He received the B.Eng. degree in electrical engineering and automation from Beijing Jiaotong University, Beijing, China, in 2018, where he is currently pursuing the Ph.D. degree in power electronics and ac drives.

RUICHANG QIU was born in Henan, China, in 1968. He received the B.S. degree in electrical engineering and automation, in 1993.

From 1990 to 2005, he worked as a Lecturer with the School of Electrical Engineering, Beijing Jiaotong University, where he is currently an Associate Professor. His current research interests include intelligent detection technology, power electronics and power conversion technology, electric traction, and transmission control.

ZHIGANG LIU was born in Shandong, China, in 1961. He received the bachelor's, master's, and Ph.D. degrees in electric drive for locomotives from Beijing Jiaotong University, Beijing, China, in 1986, 1990, and 1994, respectively.

He is currently a Full Professor with the Beijing Jiaotong University. In recent years, he presided over a number of national key scientific research projects and achieved fruitful results in the field of rail transit power supply, traction control, safety prediction and control, and so on. He published a book on power electronics and spent several months as a Visiting Scholar in the U.S. and Canada. His teaching activities and research interests include power electronics circuit and systems, rail transportation traction control and safety, and so on.

Dr. Liu is the Vice Chairman of the China Electro-technical Society Rail Transport Electrical Technical Committee, and he is also an Evaluation Expert of several national key plans.